Acta Mech 232, 4485–4495 (2021)
https://doi.org/10.1007/s00707-021-03072-8

ORIGINAL PAPER

Junxiang Yang · Chaeyoung Lee · Junseok Kim

Reduction in vacuum phenomenon for the triple junction in the ternary Cahn–Hilliard model

Received: 5 May 2021 / Revised: 26 July 2021 / Accepted: 30 August 2021 / Published online: 24 September 2021

Abstract In this study, we present a modified interfacial parameter to reduce the vacuum phenomenon for the triple junction in the ternary Cahn–Hilliard (CH) equation. The triple junction is the point where three phases meet each other. In the ternary system, we interpret a position as occupied by a phase, if the concentration of the phase is larger than one-half. Therefore, it is well known that there exists a vacuum phenomenon: none of the phases exist, that is, all the concentrations are less than one-half. In the proposed method, we introduce a phase-dependent interfacial coefficient that has a constant value away from the triple junction and smaller values in the neighborhood of the triple junction, which effectively reduces the vacuum region. To validate the superiority of the proposed approach, we present the characteristic numerical experiments for the ternary system. The computational results confirm the superior performance of the proposed method over the conventional method.

1 Introduction

A wide range of important and practical industrial processes involves multiphase liquids such as oil-water-gas multiphase fluid flows in the petroleum industry, generation of double emulsions by a microcapillary system, and droplet dynamics in microfluid or turbulent flows [1–8]. To model a three-phase system, the ternary Cahn–Hilliard (CH) system [9–18] has been successfully adopted. Furthermore, several efficient and accurate numerical methods exist for ternary CH systems [19–28].

In the ternary system, we introduce continuous order parameters $c_1(\mathbf{x}, t)$, $c_2(\mathbf{x}, t)$, and $c_3(\mathbf{x}, t)$ to represent the concentration of each phase, and require the concentrations to satisfy $c_1(\mathbf{x}, t) + c_2(\mathbf{x}, t) + c_3(\mathbf{x}, t) = 1$. However, the concentrations are $c_1(\mathbf{x}, t) = c_2(\mathbf{x}, t) = c_3(\mathbf{x}, t)$ at the triple junction points, which results in $c_1(\mathbf{x}, t) = c_2(\mathbf{x}, t) = c_3(\mathbf{x}, t) = 1/3$. Therefore, if we interpret the dominating phase domain on the space as a region of greater than one-half concentration, then we may intrinsically have a vacuum phenomenon (none of the phases exists, i.e., all the concentrations are less than one-half) around the triple junction points, as illustrated in Fig. 1.

In this study, we present a modified interfacial parameter to reduce the vacuum phenomenon for the triple junction in the ternary CH equation. In the proposed method, we introduce a phase-dependent interfacial coefficient which has similar values away from the triple junction and small values in the neighborhood of the triple junction, which effectively reduces the vacuum region. To evaluate the performance of the proposed approach, we present the characteristic numerical experiments for the ternary system.

The outline of this paper is as follows. In Sect. 2, we present a new ternary CH system. In Sect. 3, we describe the numerical solution algorithm for the ternary CH system. The numerical tests are presented in Sect. 4. The conclusions are given in Sect. 5.

J. Yang · C. Lee · J. Kim (✉)
Department of Mathematics, Korea University, Seoul 02841, Republic of Korea
E-mail: cfdkim@korea.ac.kr

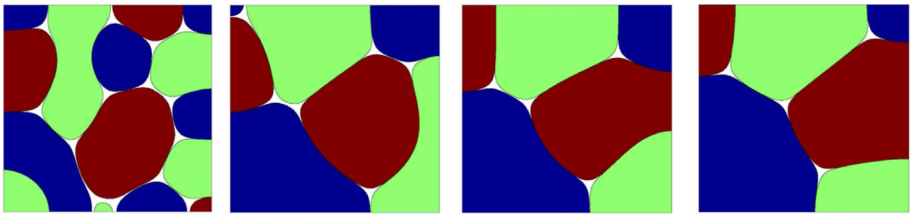

Fig. 1 Temporal evolution of concentrations in a ternary system. The filled contour lines are at the one-half level set of each phase. Reprinted from Lee et al. [29] with permission from MDPI

2 Proposed ternary CH system

Let c_l for $l = 1, 2, 3$ represent the concentration of each phase in the ternary system. The value of c_l is approximately 1 in the l-th phase, and 0 in the other phases. The variables c_1, c_2, and c_3 are required to satisfy the following hyperplane line constraint at $\mathbf{x}$ and t:

$$c_1(\mathbf{x}, t) + c_2(\mathbf{x}, t) + c_3(\mathbf{x}, t) = 1, \tag{1}$$

where $\mathbf{x} \in \Omega$ is the spatial variable, and t is the temporal variable. Here, Ω is the computational domain. The governing equations for the ternary CH system are indicated as follows:

$$\frac{\partial c_l}{\partial t} = \frac{M}{\Sigma_l}\Delta\mu_l, \tag{2}$$

$$\mu_l = \frac{12 f(c_l)}{\epsilon^2} - \frac{3}{4}\Sigma_l \Delta c_l + \frac{12\beta(\mathbf{c})}{\epsilon^2}, \quad l = 1, 2, 3, \tag{3}$$

where Σ_l is a parameter related to the interfacial force, and ϵ is a positive interfacial coefficient, related to the thickness of the diffuse interface [30]. In previous studies [13,14,19,21,24,29,30], ϵ was taken as constant, μ_l is the chemical potential of the l-th phase, $F(\mathbf{c}) = \sum_{l=1}^{3} 0.5\Sigma_l c_l^2(c_l - 1)^2 + 3\Gamma c_1^2 c_2^2 c_3^3$ is the nonlinear potential and $\Gamma \geq 0$, $f(c_i) = \partial F(\mathbf{c})/\partial c_l$, $\beta(\mathbf{c}) = -\frac{1}{\Sigma_T}\sum_{l=1}^{3} f(c_l)/\Sigma_l$ [30] is the Lagrange multiplier, which is utilized to satisfy the constraint (1), $1/\Sigma_T = \sum_{l=1}^{3} 1/\Sigma_l$. In this study, we adopt the periodic or the following zero Neumann boundary conditions:

$$\nabla c_l \cdot \mathbf{n}|_{\partial\Omega} = \nabla\mu_l \cdot \mathbf{n}|_{\partial\Omega} = 0, \quad l = 1, 2, 3,$$

where $\mathbf{n}$ is the normal vector to the domain boundary $\partial\Omega$.

To reduce the vacuum phenomenon, as illustrated in Fig. 1, we propose a new phase-dependent interfacial coefficient which has a similar value away from the triple junction and small values in the neighborhood of the triple junction, which effectively reduces the vacuum region. The proposed phase-dependent interfacial coefficient is defined as

$$\epsilon(c_1, c_2, c_3) = \epsilon_0(1 - s\, c_1 c_2 c_3), \tag{4}$$

where ϵ_0 is a predefined positive constant and s is a scaling factor that satisfies $0 < s < 27$. When $s = 0$, the phase-dependent interfacial coefficient becomes a constant coefficient, ϵ_0. Because the maximum value of $c_1 c_2 c_3$ is $1/27$, we require $s < 27$ to have positive values of $\epsilon(c_1, c_2, c_3)$. Owing to the constraint $c_1 + c_2 + c_3 = 1$, we solve only the equations for c_1 and c_2, that is,

$$\frac{\partial c_1}{\partial t} = \frac{M}{\Sigma_1}\Delta\mu_1, \tag{5}$$

$$\mu_1 = \frac{12f(c_1)}{\epsilon^2(c_1,c_2,c_3)} - \frac{3}{4}\Sigma_1\Delta c_1 - \frac{12\beta(\mathbf{c})}{\epsilon^2(c_1,c_2,c_3)}, \tag{6}$$

$$\frac{\partial c_2}{\partial t} = \frac{M}{\Sigma_2}\Delta\mu_2, \tag{7}$$

$$\mu_2 = \frac{12f(c_2)}{\epsilon^2(c_1,c_2,c_3)} - \frac{3}{4}\Sigma_2\Delta c_2 - \frac{12\beta(\mathbf{c})}{\epsilon^2(c_1,c_2,c_3)}. \tag{8}$$

After c_1 and c_2 are computed, we can directly get $c_3 = 1 - c_1 - c_2$.

3 Numerical solution

Here we present the numerical scheme of a two-dimensional computational domain, $\Omega = (a,b)\times(c,d)$. Let $h = (b-a)/N_x = (d-c)/N_y$ be the uniform grid size, where N_x and N_y are positive even integers. Then, $\Omega_h = \{(x_i,y_j) : x_i = a + (i-0.5)h,\ y_j = c + (j-0.5)h,\ 1 \le i \le N_x,\ 1 \le j \le N_y\}$ is the discrete computational domain. In addition, let $c^n_{l,ij}$ and $\mu^n_{l,ij}$ be approximations of $c_l(x_i,y_j,n\Delta t)$ and $\mu_l(x_i,y_j,n\Delta t)$ with time level n, where Δt is the time step size. We adopt a stabilized semi-implicit scheme to discretize Eqs. (5)–(8) in time. Spatial discretization is performed using the standard finite difference method. The fully discrete governing equations are given by

$$\frac{c^{n+1}_{1,ij} - c^n_{1,ij}}{\Delta t} = \frac{M}{\Sigma_1}\Delta\mu^{n+1}_{1,ij}, \tag{9}$$

$$\begin{aligned}\mu^{n+1}_{1,ij} = {} & \frac{12f(c^n_{1,ij})}{\epsilon^2(c^n_{1,ij},c^n_{2,ij},c^n_{3,ij})} - \frac{3}{4}\Sigma_1\Delta_h c^{n+1}_{1,ij} + \frac{12\beta(\mathbf{c}^n_{ij})}{\epsilon^2(c^n_{1,ij},c^n_{2,ij},c^n_{3,ij})} \\ & + \frac{S\Sigma_1(c^{n+1}_{1,ij} - c^n_{1,ij})}{\epsilon^2(c^n_{1,ij},c^n_{2,ij},c^n_{3,ij})},\end{aligned} \tag{10}$$

$$\frac{c^{n+1}_{2,ij} - c^n_{2,ij}}{\Delta t} = \frac{M}{\Sigma_2}\Delta\mu^{n+1}_{1,ij}, \tag{11}$$

$$\begin{aligned}\mu^{n+1}_{2,ij} = {} & \frac{12f(c^n_{2,ij})}{\epsilon^2(c^n_{1,ij},c^n_{2,ij},c^n_{3,ij})} - \frac{3}{4}\Sigma_2\Delta_h c^{n+1}_{2,ij} + \frac{12\beta(\mathbf{c}^n_{ij})}{\epsilon^2(c^n_{1,ij},c^n_{2,ij},c^n_{3,ij})} \\ & + \frac{S\Sigma_2(c^{n+1}_{2,ij} - c^n_{2,ij})}{\epsilon^2(c^n_{1,ij},c^n_{2,ij},c^n_{3,ij})},\end{aligned} \tag{12}$$

where $S > 0$ is the stabilization parameter and the discrete Laplacian of a specific function ψ is defined as $\Delta_h\psi_{ij} = (\psi_{i+1,j} + \psi_{i-1,j} - 4\psi_{ij} + \psi_{i,j+1} + \psi_{i,j-1})/h^2$. At the discrete boundary $\partial\Omega_h$, we utilize the periodic or the following discrete zero Neumann boundary conditions as follows:

$$\begin{aligned}
&c^{n+1}_{1,0j} = c^{n+1}_{1,1j},\ c^{n+1}_{1,N_x+1,j} = c^{n+1}_{1,N_x,j},\ c^{n+1}_{1,i0} = c^{n+1}_{1,i1},\ c^{n+1}_{1,iN_y+1} = c^{n+1}_{1,iN_y},\\
&\mu^{n+1}_{1,0j} = \mu^{n+1}_{1,1j},\ \mu^{n+1}_{1,N_x+1,j} = \mu^{n+1}_{1,N_x,j},\ \mu^{n+1}_{1,i0} = \mu^{n+1}_{1,i1},\ \mu^{n+1}_{1,iN_y+1} = \mu^{n+1}_{1,iN_y},\\
&c^{n+1}_{2,0j} = c^{n+1}_{2,1j},\ c^{n+1}_{2,N_x+1,j} = c^{n+1}_{2,N_x,j},\ c^{n+1}_{2,i0} = c^{n+1}_{2,i1},\ c^{n+1}_{2,iN_y+1} = c^{n+1}_{2,iN_y},\\
&\mu^{n+1}_{2,0j} = \mu^{n+1}_{2,1j},\ \mu^{n+1}_{2,N_x+1,j} = \mu^{n+1}_{2,N_x,j},\ \mu^{n+1}_{2,i0} = \mu^{n+1}_{2,i1},\ \mu^{n+1}_{2,iN_y+1} = \mu^{n+1}_{2,iN_y}.
\end{aligned}$$

Here we adopt the nonlinear multigrid method with a Gauss–Seidel relaxation [31] to solve the discrete systems (9)–(10) and (11)–(12) separately. Please refer to [32] for the details of the multigrid method. It is easy to obtain $c^{n+1}_{3,ij} = 1 - c^{n+1}_{1,ij} - c^{n+1}_{2,ij}$ with the updated $c^{n+1}_{1,ij}$ and $c^{n+1}_{2,ij}$. The numerical procedure in one iteration is completed.

4 Numerical experiments

We validate the performance of the proposed model by adopting various computational experiments such as triple junction, ternary phase separation, liquid lens, raising bubble, and pressure jump. In the following simulations, we choose $\Sigma_1 = \Sigma_2 = \Sigma_3 = 1$, $\Gamma = 0.1$, and $S = 20$; and the discrete homogeneous Neumann boundary condition unless otherwise specified.

4.1 Triple junction

First, we validate the proposed model by investigating the evolution of the triple junction. The following initial conditions on $\Omega = (0, 1) \times (0, 1)$ are used:

$$c_1(x, y, 0) = \begin{cases} 1, & \text{if } x < 0.5 \text{ and } y > 0.4, \\ 0, & \text{otherwise,} \end{cases}$$
$$c_2(x, y, 0) = \begin{cases} 1, & \text{if } x > 0.5 \text{ and } y > 0.4, \\ 0, & \text{otherwise,} \end{cases}$$
$$c_3(x, y, 0) = 1 - c_1(x, y, 0) - c_2(x, y, 0).$$

We use $\Delta t = 0.01$, $M = 0.01$, and $h = 1/128$. For the CH-type phase-field model, a small and positive interfacial coefficient ϵ_0 controls the evolutionary dynamics of the interface. In general, a relatively large and appropriate ϵ_0 is required to obtain smooth interfacial dynamics. However, the vacuum phenomenon is always observed if relatively large ϵ_0 is utilized (see Fig. 1). Although a smaller ϵ_0 can be used to reduce the vacuum phenomenon, the evolution of the interface will be pinned, because the strong nonlinearity increases the stiffness of the problem. In this test, we aim to illustrate that the proposed model can reduce the vacuum phenomenon with a relatively large ϵ_0. To perform the comparison, we set three pairs as $(s, \epsilon_0) = (0, 0.036)$, $(0, 0.018)$, and $(25, 0.036)$, where $s = 0$ represents the cases with constant interfacial coefficient. Figure 2a illustrates the snapshots at $t = 8$ with $s = 0$ and $\epsilon_0 = 0.036$. In this case, the interfacial coefficient $\epsilon(c_1, c_2, c_3) = c_0$ is constant. We can observe that a vacuum phenomenon appears. As illustrated in Fig. 2b, we display the result with $s = 0$ and $\epsilon_0 = 0.018$. Although the vacuum phenomenon is reduced by using a smaller value of ϵ_0, the evolutionary dynamics is pinned. In Fig. 2c, the result with $s = 25$ and $\epsilon_0 = 0.036$ indicates that the proposed method not only captures the interfacial dynamics but also significantly reduces the vacuum phenomenon. In Fig. 2d–f, we display the evolutions of mass with respect to $(s, \epsilon_0) = (0, 0.036)$, $(0, 0.018)$, and $(25, 0.036)$, respectively. It can be observed that the mass of each component is conserved, even if a non-constant interfacial coefficient is used.

Next, we consider the initial conditions with randomly distributed values of c_1, c_2, and c_3. Here, the parameter values are the same as those of the previous test. The top and bottom rows of Fig. 3 display the computational results with $s = 0$ and $s = 25$ at different computational moments. Evidently, the proposed model reduces the vacuum phenomenon at triple junctions and three components arrive at a regular state, where the contact angle is approximately 120°.

4.2 Ternary phase separation

Phase separation is a basic benchmark problem for the ternary CH model. In a homogeneous ternary mixture, the concentration fluctuations grow with time and lead to the formation of three-component state. In this test, we consider the initial conditions on $\Omega = (0, 1) \times (0, 1)$ as follows:

$$c_1(x, y, 0) = \frac{1}{3} + 0.01\text{rand}(x, y), \quad c_2(x, y, 0) = \frac{1}{3} + 0.01\text{rand}(x, y),$$
$$c_3(x, y, 0) = 1 - c_1(x, y, 0) - c_2(x, y, 0),$$

where $\text{rand}(x, y)$ is a random number in $[-1, 1]$. We use $h = 1/128$, $\Delta t = 0.01$, $M = 0.01$, and $\epsilon_0 = 0.036$. The top row of Fig. 4 shows the computational results at $t = 0.8$ with $s = 0$, $s = 18$, and $s = 25$, respectively. We discover that the vacuum phenomenon is significantly reduced as the value of s is increased. In the bottom row of Fig. 4, we plot the evolutions of mass with respect to $s = 0,\ 18,\ 25$. We observe that the mass of each phase is conserved even if the non-constant interfacial coefficient is adopted.

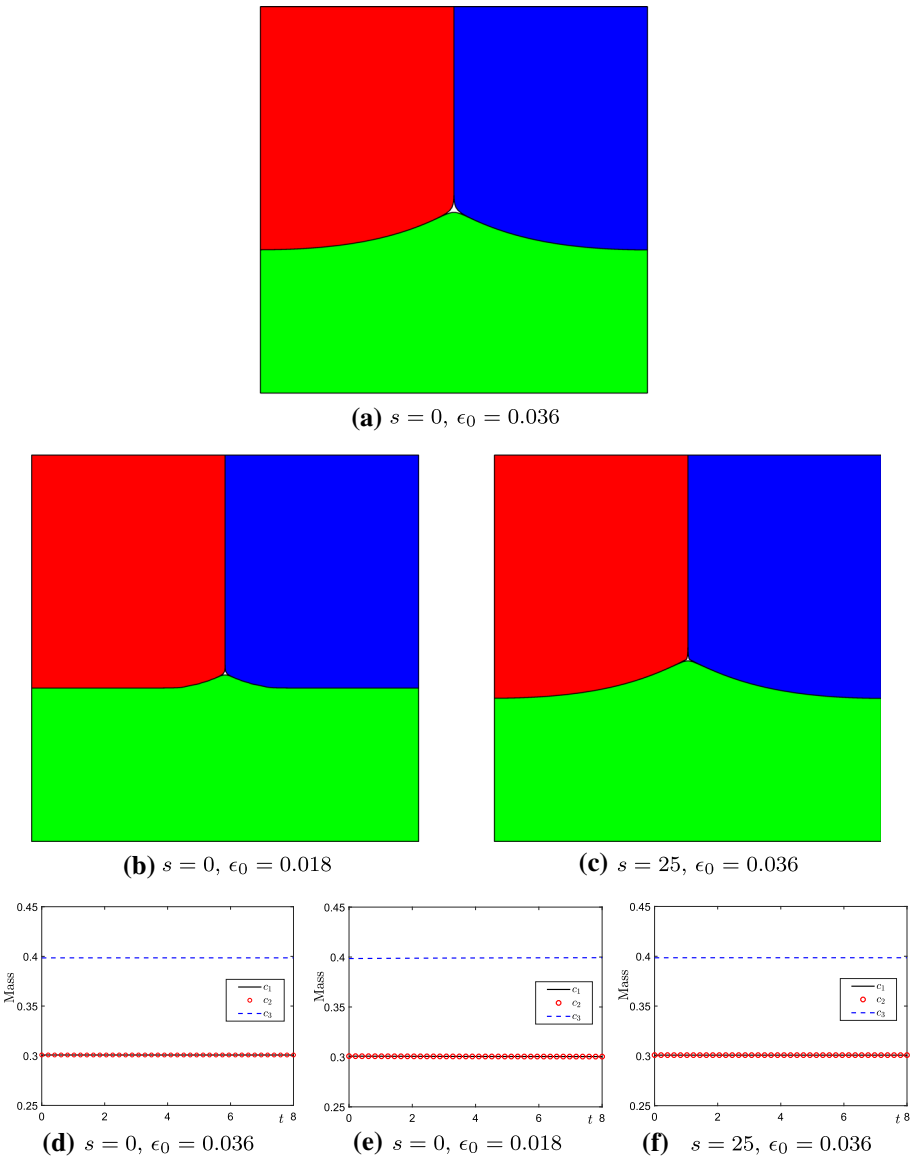

(a) $s = 0,\ \epsilon_0 = 0.036$

(b) $s = 0,\ \epsilon_0 = 0.018$ **(c)** $s = 25,\ \epsilon_0 = 0.036$

(d) $s = 0,\ \epsilon_0 = 0.036$ **(e)** $s = 0,\ \epsilon_0 = 0.018$ **(f)** $s = 25,\ \epsilon_0 = 0.036$

Fig. 2 Triple junction with **a** $s = 0$, $\epsilon_0 = 0.036$; **b** $s = 0$, $\epsilon_0 = 0.018$; and **c** $s = 25$, $\epsilon_0 = 0.036$. Here, the red, blue, and green regions are occupied by c_1, c_2, and c_3, respectively. Here, **d–f** illustrate the evolution of mass of each phase.

4.3 Liquid lens

In this section, we consider a liquid lens with a phase-dependent interfacial coefficient. The component c_1 initially occupies the circular region which is located at the interface of the components c_2 and c_3. With the temporal evolution of interfaces, the circular region occupied by c_1 is elongated, owing to the interfacial force. The initial conditions on $\Omega = (0, 1) \times (0, 1)$ are defined as follows:

$$
\begin{aligned}
c_3(x, y, 0) &= 0.5 + 0.5 \tanh\left(\frac{0.2 - \sqrt{(x-0.5)^2 + (y-0.5)^2}}{2\sqrt{2}\epsilon_0}\right),\\
c_1(x, y, 0) &= (1 - c_3(x, y, 0))\left(0.5 + 0.5 \tanh\left(\frac{y - 0.5}{2\sqrt{2}\epsilon_0}\right)\right),\\
c_2(x, y, 0) &= 1 - c_1(x, y, 0) - c_3(x, y, 0).
\end{aligned}
$$

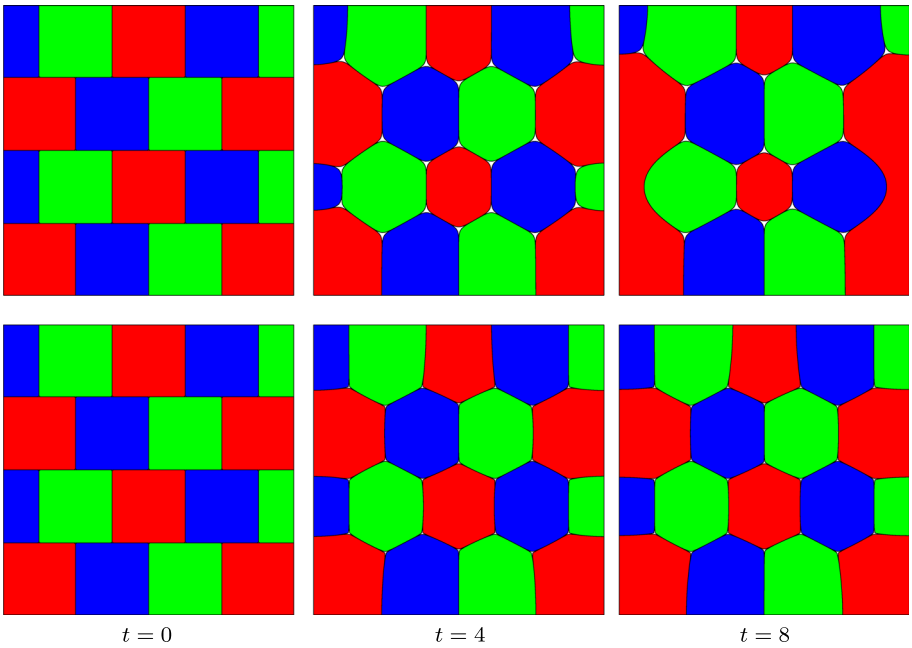

Fig. 3 Temporal evolution of the triple junctions: top row ($s = 0$) and bottom row ($s = 25$). Here, the red, blue, and green regions are occupied by c_1, c_2, and c_3, respectively

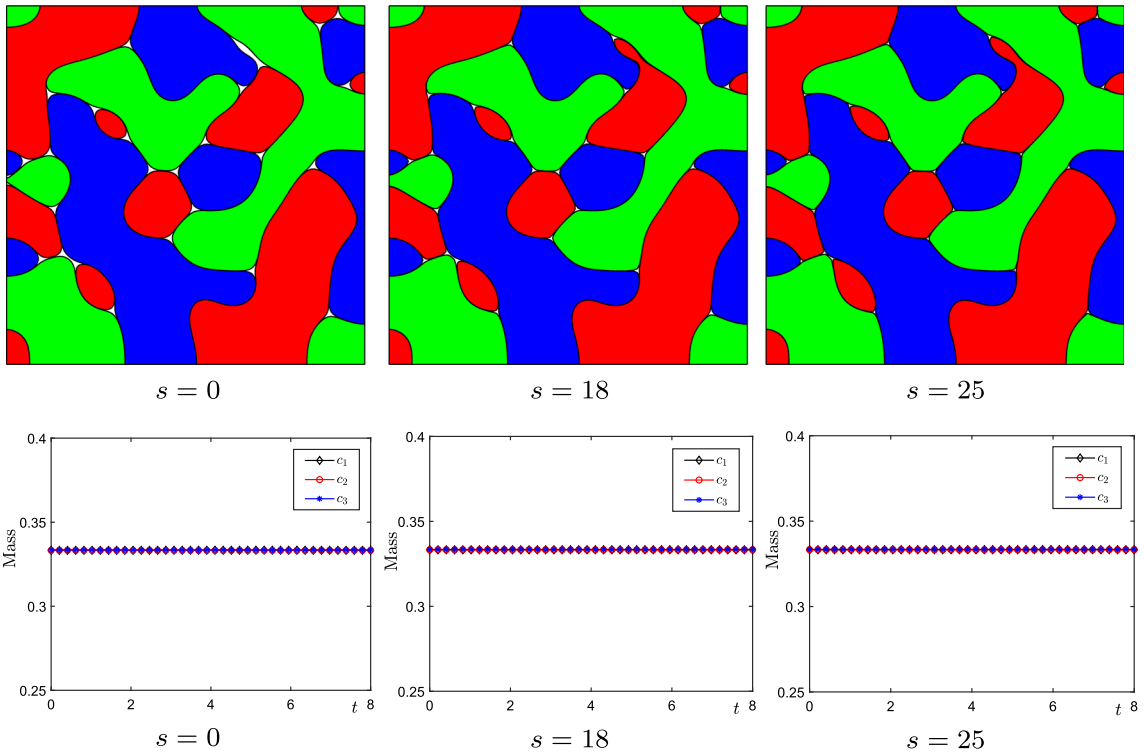

Fig. 4 Phase separation with different phase-dependent interfacial coefficients. Here, the red, blue, and green regions are occupied by c_1, c_2, and c_3, respectively. The bottom row displays the evolution of mass of each phase

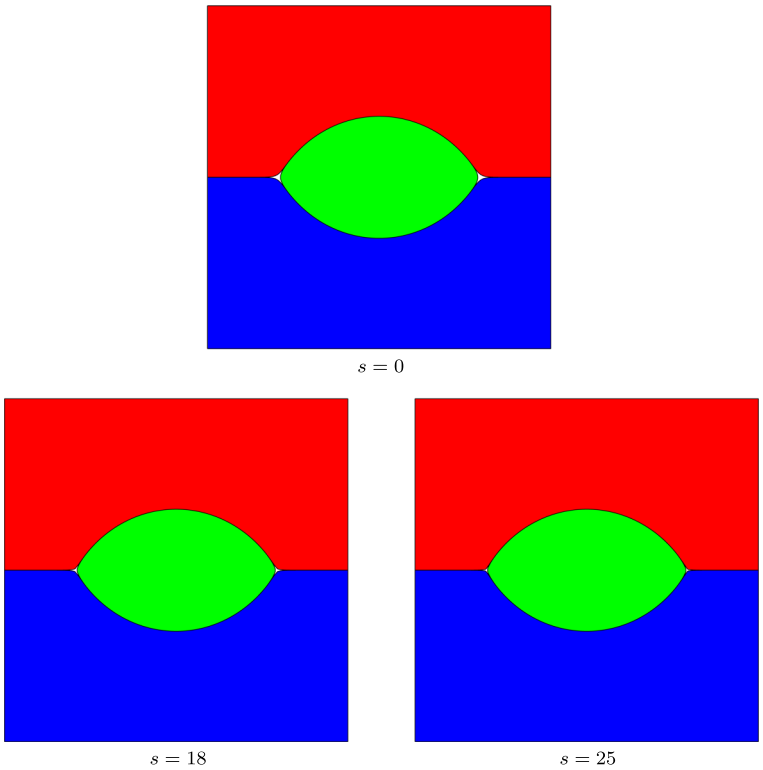

Fig. 5 Liquid lens at $t = 8$ with different phase-dependent interfacial coefficients. Here, the red, blue, and green regions are occupied by c_1, c_2, and c_3, respectively

here we use $h = 1/128$, $\Delta t = 0.01$, $M = 0.01$, and $\epsilon_0 = 0.036$. In Fig. 5, we show the snapshots at $t = 8$ with different values of $s = 0$, $s = 18$, and $s = 25$. Evidently, our proposed model obviously reduces the vacuum phenomenon with an increase of s.

4.4 Raising bubble with fluid flow

In this subsection, we investigate the rising bubble in ternary fluid system. The dimensionless governing equations consist of the convective ternary CH model and incompressible Navier–Stokes (NS) model as follows:

$$\frac{\partial c_l}{\partial t} + \nabla \cdot (c_l \mathbf{u}) = \frac{1}{Pe\Sigma_l} \Delta \mu_l, \tag{13}$$

$$\mu_l = \frac{12F'(c_l)}{\epsilon^2} - \frac{3}{4}\Sigma_l \Delta c_l + \frac{12\beta(\mathbf{c})}{\epsilon^2}, \quad l = 1, 2, 3, \tag{14}$$

$$\rho(\mathbf{c})\left(\frac{\partial \mathbf{u}}{\partial t} + \mathbf{u} \cdot \nabla \mathbf{u}\right) = -\nabla p + \frac{1}{Re}\nabla \cdot [\eta(\mathbf{c})(\nabla \mathbf{u} + \nabla \mathbf{u}^T)] + SF(\mathbf{c}) + \frac{\rho(\mathbf{c})}{Fr^2}\mathbf{g}, \tag{15}$$

$$\nabla \cdot \mathbf{u} = 0, \tag{16}$$

where $\mathbf{u} = (u, v)$ is the velocity field, u and v are the velocity components along the x- and y-directions, respectively, p is the pressure, $\rho(\mathbf{c}) = \sum_{l=1}^{3} \rho_l c_l$ is the density of the entire system, and $\eta(\mathbf{c}) = \sum_{l=1}^{3} \eta_l c_l$ is the viscosity of the entire system. Here, ρ_l and η_l are the density and viscosity of the l-th phase, respectively.

Gravity is $\mathbf{g} = (0, -g)$. The continuous surface tension of the ternary system is [33]

$$SF(\mathbf{c}) = -\sum_{l=1}^{3} \frac{1}{We_l} \nabla \cdot \left(\frac{\nabla c_l}{|\nabla c_l|} \right) \nabla c_l = \sum_{l=1}^{3} \frac{1}{We_l} \nabla \cdot \left(-\frac{\nabla c_l}{|\nabla c_l|} \right) |\nabla c_l| \frac{\nabla c_l}{|\nabla c_l|}, \tag{17}$$

where $\nabla \cdot (-\nabla c_l/|\nabla c_l|)$ is the curvature, $|\nabla c_l|$ is the Dirac delta function [34], $\nabla c_l/|\nabla c_l|$ is the unit normal vector to the interface. The dimensionless parameters are the Reynolds number Re, Peclet number Pe, Weber numbers We_l and $l = 1, 2, 3$, and the Froude number Fr. To numerically solve the incompressible NS model, Eqs. (15) and (16), we adopt the projection method with pressure correction. For some details of the implementation of the projection method, please refer to [35,36]. Along the x-direction, we apply the periodic boundary condition for all variables. The homogeneous Neumann boundary condition is considered along the y-direction.

Numerical tests are performed on $\Omega = (0, 2) \times (0, 4)$. The initial conditions are as follows:

$$\begin{aligned}
c_1(x, y, 0) &= 0.5 + 0.5 \tanh \left(\frac{0.3 - \sqrt{(x-1)^2 + (y-1.62)^2}}{2\sqrt{2}\epsilon_0} \right), \\
c_2(x, y, 0) &= (1 - c_1(x, y, 0)) \left(0.5 + 0.5 \tanh \left(\frac{y-2}{2\sqrt{2}\epsilon_0} \right) \right), \\
c_3(x, y, 0) &= 1 - c_1(x, y, 0) - c_2(x, y, 0), \\
u(x, y, 0) &= v(x, y, 0) = p(x, y, 0) = 0.
\end{aligned}$$

Here we use $h = 1/64$, $\Delta t = 2.4414\text{e-}3$, $\epsilon_0 = 0.048$, $Re = 100$, $Pe = 40000/\epsilon_0$, $We_1 = 7.5$, $We_2 = 10$, $We_3 = 5$, $Fr = 1$, $g = 1$, the density ratio is $\rho_1 : \rho_2 : \rho_3 = 1 : 3 : 5$, the viscosity ratio is $\eta_1 : \eta_2 : \eta_3 = 1 : 1 : 1$. In Fig. 6, we display the computational results with different values of $s = 0$ and $s = 25$ at different computational moments. It can be observed that the proposed model with phase-dependent interfacial coefficient obviously reduces the vacuum phenomenon. Figure 7 displays the evolution of mass of each phase with respect to $s = 0$ and $s = 25$. It can be observed that mass conservation is satisfied.

4.5 Pressure jump

Finally, we investigate the pressure distribution, which is widely used as the benchmark problem for multiphase fluid system [33]. With the absence of fluid viscosity, gravity, and other external forces, the Laplace formula [33] gives $[p] = \sigma\kappa$, where $[p]$ is the pressure jump near the interface, σ is the surface tension coefficient, and κ is the curvature. For a circular droplet, we have $[p] = \sigma\kappa = \sigma/R$, where R is the radius. For a ternary system with the surface tension formula (17), we have $\sigma_{mn} = 1/We_m + 1/We_n$ [33], where σ_{mn} is the surface tension coefficient between fluid m and fluid n. The decomposition can be expressed as follows:

$$\frac{1}{We_1} = \frac{\sigma_{12} + \sigma_{13} - \sigma_{23}}{2}, \quad \frac{1}{We_2} = \frac{\sigma_{12} + \sigma_{23} - \sigma_{13}}{2}, \frac{1}{We_3} = \frac{\sigma_{13} + \sigma_{23} - \sigma_{12}}{2}.$$

In this test, the domain is set to be $\Omega = (0, 2) \times (0, 1)$. The initial conditions are defined as

$$c_1(x, y, 0) = 0.5 + 0.5 \tanh \left(\frac{0.15 - \sqrt{(x-0.5)^2 + (y-0.5)^2}}{2\sqrt{2}\epsilon_0} \right), \tag{18}$$

$$c_1(x, y, 0) = 0.5 + 0.5 \tanh \left(\frac{0.15 - \sqrt{(x-1.5)^2 + (y-0.5)^2}}{2\sqrt{2}\epsilon_0} \right), \tag{19}$$

$$c_3(x, y, 0) = 1 - c_1(x, y, 0) - c_2(x, y, 0), \tag{20}$$

$$u(x, , y, 0) = v(x, y, 0) = p(x, y, 0) = 0. \tag{21}$$

Figure 8a illustrates the initial stage. Here, we use $h = 1/512$, $\Delta t = 3.8147\text{e-}5$, $\epsilon_0 = 0.0038$, $Re = 1$, $Pe = 1/\epsilon_0$, $\sigma_{12} = 1$, $\sigma_{13} = 0.75$, $\sigma_{23} = 1.5$. In Fig. 8b, the distribution of pressure is plotted. From the Laplace formula, the exact pressure jumps are $[p] = 5$ and $[p] = 10$. The numerical and exact pressure jumps at $y = 0.5$ are plotted in Fig. 8c, we discover that the computational and exact results are in good agreement with each other.

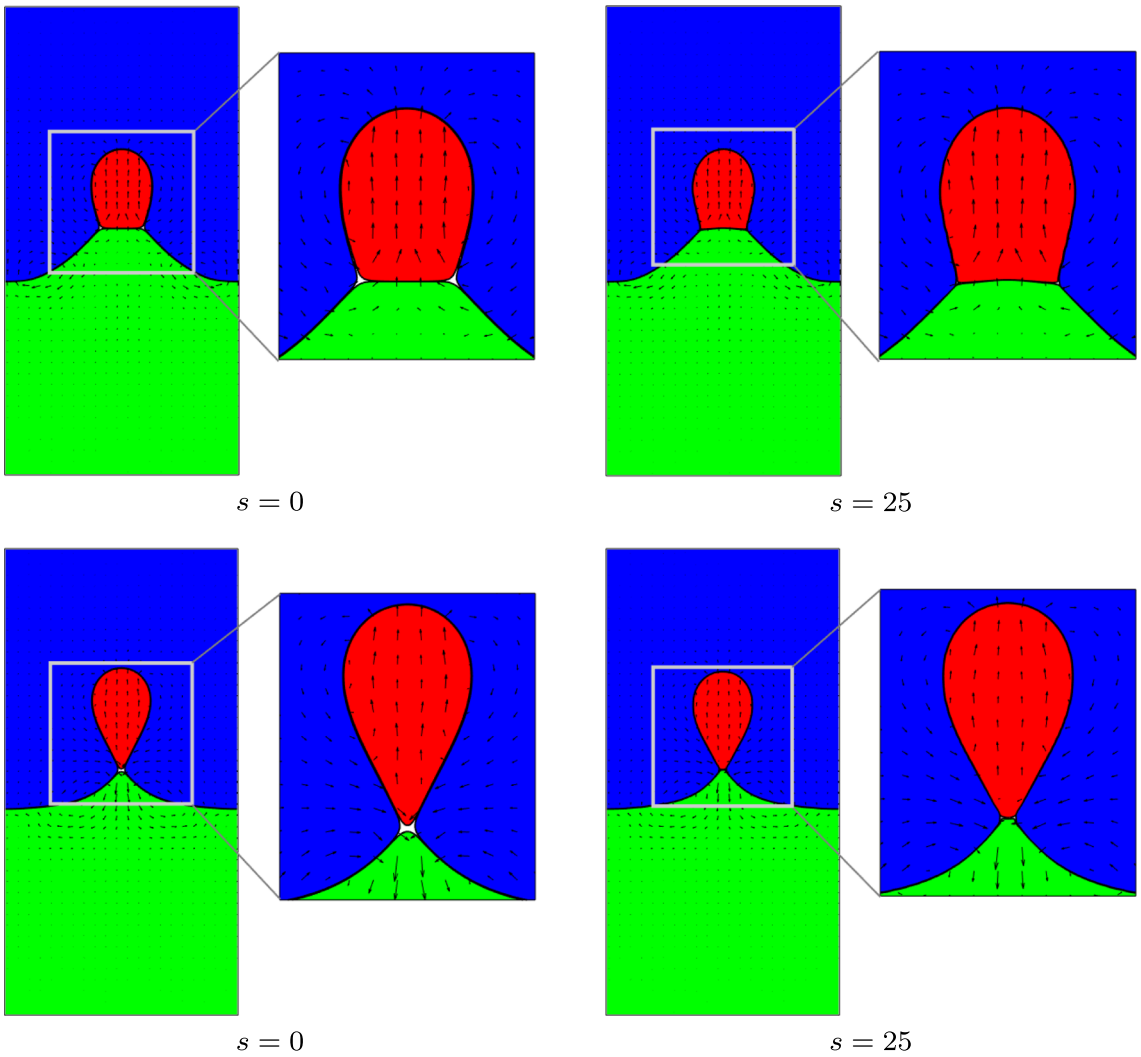

Fig. 6 Raising bubble in a ternary fluid system. Here, the red, blue, and green regions are occupied by c_1, c_2, and c_3, respectively. The top and bottom rows illustrate the snapshots at $t = 3.66$ and $t = 4.88$

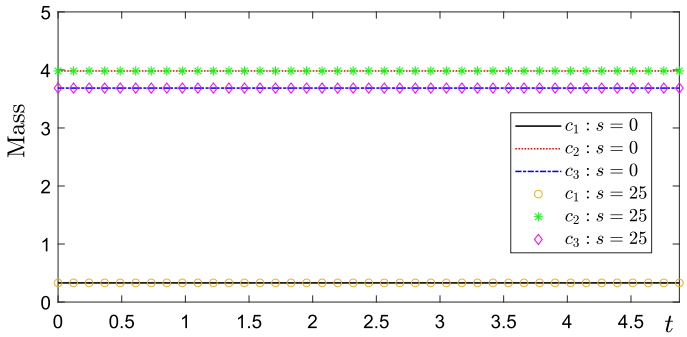

Fig. 7 Evolutions of the mass of each phase with respect to $s = 0$ and $s = 25$

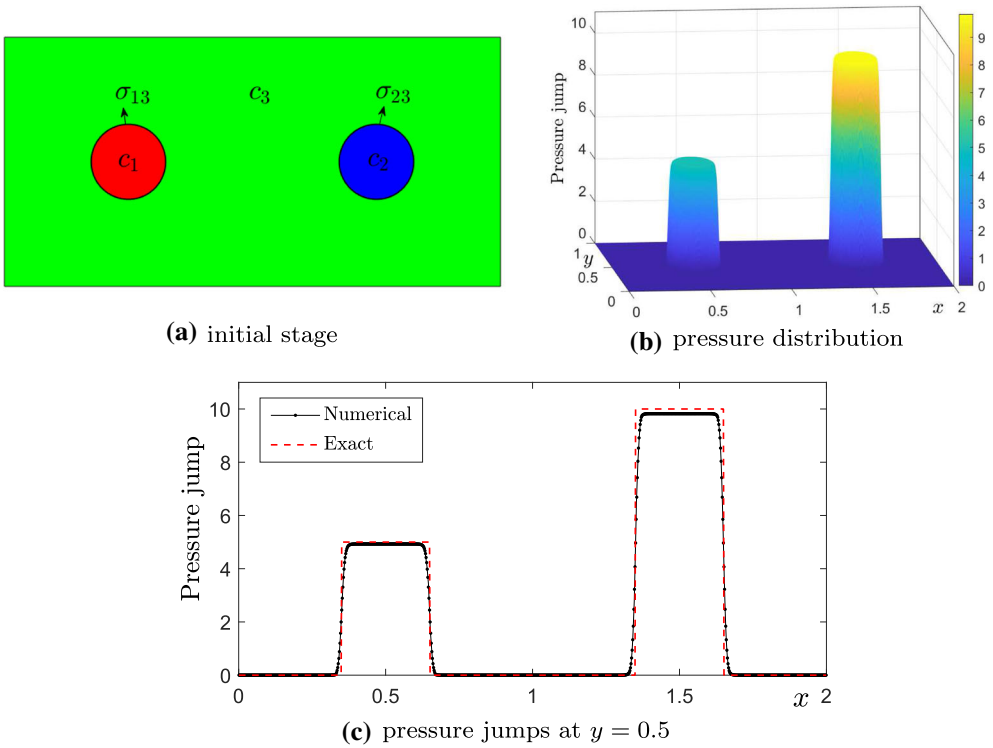

(a) initial stage **(b)** pressure distribution

(c) pressure jumps at $y = 0.5$

Fig. 8 Pressure distribution in a ternary system. Here, **a**, **b**, and **c** are initial state, pressure distribution, and pressure jumps at slice $y = 0.5$

5 Conclusions

In this study, we proposed a novel ternary CH system with a phase-dependent interfacial coefficient. In contrast to the constant interfacial coefficient used in previous researches [13,14,19,21,24,29,30], the present model has a similar value of interfacial coefficient away from the triple junction and small values in the neighborhood of the triple junction. Various numerical experiments indicated that the vacuum phenomenon is significantly reduced. In future studies, we will extend the ternary CH system to the N-component CH system, ($N > 3$). We may use $\epsilon(c_1, \cdots, c_N) = \epsilon_0(1 - s \sum_{1 \le p < q < r \le N} c_p c_q c_r)$, $0 < s < 27$ for the phase-dependent interfacial coefficient in the N-component CH system.

Acknowledgements The corresponding author (J. S. Kim) was supported by the National Research Foundation (NRF), Korea, under Project BK21 FOUR. The authors thank the reviewers for their constructive comments regarding the revision of this article.

References

1. Shi, J., Cheng, L., Cao, R., Jia, Z., Liu, G.: Phase-field simulation of imbibition for the matrix-fracture of tight oil reservoirs considering temperature change. Water **13**(7), 1004 (2021)
2. Park, J.M., Anderson, P.D.: A ternary model for double-emulsion formation in a capillary microfluidic device. Lab Chip **12**, 2672–2677 (2012)
3. Fu, Y., Zhao, S., Bai, L., Jin, Y., Cheng, Y.: Numerical study of double emulsion formation in microchannels by a ternary Lattice Boltzmann method. Chem. Eng. Sci. **146**, 126–134 (2016)
4. Azarmanesh, M., Farhadi, M., Azizian, P.: Double emulsion formation through hierarchical flow-focusing microchannel. Phys. Fluid **28**, 032005 (2016)
5. Wang, N., Semprebon, C., Liu, H., Zhang, C., Kusumaatmaja, H.: Modelling double emulsion formation in planar flow-focusing microchannels. J. Fluid Mech. **895**, A22 (2002)
6. Wörner, M., Samkhaniani, N., Cai, X., Wu, Y., Majumdar, A., Marschall, H., Frohnapfel, B., Deutschmann, O.: Spreading and rebound dynamics of sub-millimetre urea-water-solution droplets impinging on substrates of varying wettability. Appl. Math. Model **95**, 53–73 (2021)
7. Shin, J., Yang, J., Lee, C., Kim, J.: The Navier–Stokes–Cahn–Hilliard model with a high-order polynomial free energy. Acta Mech. **231**, 2425–2437 (2020)

8. Soligo, G., Roccon, A., Soldati, A.: Mass-conservation-improved phase field methods for turbulent multiphase flow simulation. Acta Mech. **230**, 683–696 (2019)
9. Lee, H.G., Kim, J.: An efficient numerical method for simulating multiphase flows using a diffuse interface model. Physica A **423**, 33–50 (2015)
10. Liang, H., Shi, B.C., Chai, Z.H.: Lattice Boltzmann modeling of three-phase incompressible flows. Phys. Rev. E **93**, 013308 (2016)
11. Liang, H., Xu, J., Chen, J., Chai, Z., Shi, B.: Lattice Boltzmann modeling of wall-bounded ternary fluid flows. Appl. Math. Model **73**, 487–513 (2019)
12. Fakhari, A., Bolster, D.: Diffuse interface modeling of three-phase contact line dynamics on curved boundaries: a lattice Boltzmann model for large density and viscosity ratios. J. Comput. Phys. **334**, 620–638 (2017)
13. Li, H.-L., Liu, H.-R., Ding, H.: A fully 3D simulation of fluid-structure interaction with dynamic wetting and contact angle hysteresis. J. Comput. Phys. **420**(1), 109709 (2020)
14. Zhang, Q., Wang, X.P.: Phase field modeling and simulation of three-phase flow on solid surfaces. J. Comput. Phys. **319**, 79–107 (2016)
15. Zhou, S., Xie, Y.M.: Numerical simulation of three-dimensional multicomponent Cahn–Hilliard systems. Int. J. Mech. Sci. **198**, 106349 (2021)
16. Haghani-Hassan-Abadi, R., Fakhari, A., Rahimian, M.H.: Numerical simulation of three-component multiphase flows at high density and viscosity ratios using lattice Boltzmann methods. Phys. Rev. E **97**, 033312 (2018)
17. Semprebon, C., Krüger, T., Kusumaatmaja, H.: Ternary free-energy lattice Boltzmann model with tunable surface tensions and contact angels. Phys. Rev. E **93**, 033305 (2016)
18. Yi, S.: A phase-field method for the numerical simulation of rigid particulate in two-phase flows. Fluid Dyn. Res. **52**, 015512 (2020)
19. Jeong, D., Yang, J., Kim, J.: A practical and efficient numerical method for the Cahn–Hilliard equation in complex domains. Commun. Nonlinear Sci. Numer. Simul. **73**, 217–228 (2019)
20. Liang, H., Zhang, C., Du, R., Wei, Y.: Lattice Boltzmann method for fractional Cahn–Hilliard equation. Commun. Nonlinear Sci. Numer. Simul. **91**, 105443 (2020)
21. Yang, J., Kim, J.: An unconditionally stable second-order accurate method for systems of Cahn–Hilliard equations. Commun. Nonlinear Sci. Numer. Simul. **87**, 105276 (2020)
22. Rohde, C., von Wolff, L.: A ternary Cahn–Hilliard–Navier–Stokes model for two-phase flow with precipitation and dissolution. Math. Model Methods Appl. Sci. **31**(1), 1–35 (2021)
23. Haghani-Hassan-Abadi, R., Rahimian, M.H.: Axisymmetric lattice Boltzmann model for simulation of ternary fluid flows. Acta Mech. **231**, 2323–2334 (2020)
24. Yang, J., Kim, J.: Linear, second-order accurate, and energy stable scheme for a ternary Cahn–Hilliard model by using Lagrange multiplier approach. Acta Appl. Math. **172**, 10 (2021)
25. Li, Y., Choi, J.-I., Kim, J.: Multi-component Cahn–Hilliard system with different boundary conditions in complex domains. J. Comput. Phys. **323**, 1–16 (2016)
26. Huang, Z., Lin, G., Ardekani, A.M.: A consistent and conservative model and its scheme for N-phase-M-component incompressible flows. J. Comput. Phys. **434**, 110229 (2021)
27. Zhu, G., Chen, H., Li, A., Sun, S., Yao, J.: Fully discrete energy stable scheme for a phase-field moving contact line model with variable densities and viscosities. Appl. Math. Model **83**, 614–639 (2020)
28. Ren, H., Zhuang, X., Trung, N.T., Rabczuk, T.: Nonlocal operator method for the Cahn–Hilliard phase field model. Commun. Nonlinear Sci. Numer. Simul. **96**, 105687 (2021)
29. Lee, H.G., Shin, J., Lee, J.-Y.: A high-order convex splitting method for a non-additive Cahn–Hilliard energy functional. Mathematics **7**(12), 1242 (2019)
30. Boyer, F., Lapuerta, C.: Study of a three component Cahn–Hilliard flow model. ESAIM Math. Model Numer. Anal. **40**(4), 653–687 (2006)
31. Trottenberg, U., Oosterlee, C., Schüller, A.: Multigrid. Academic Press, London (2001)
32. Kim, J., Kang, K., Lowengrub, J.: Conservative multigrid methods for Cahn–Hilliard fluids. J. Comput. Phys. **193**(2), 511–543 (2004)
33. Kim, J.: Phase field computations for ternary fluid flows. Comput. Methods Appl. Mech. Eng. **196**, 4779–4788 (2007)
34. Lee, H.G., Kim, J.: Regularized Dirac delta functions for phase field models. Int. J. Numer. Methods Eng. **91**, 269–288 (2012)
35. Chorin, A.J.: A numerical method for solving incompressible viscous flow problems. J. Comput. Phys. **2**, 12–26 (1967)
36. Yang, J., Kim, J.: A phase-field model and its efficient numerical method for two-phase flows on arbitrarily curved surfaces in 3D space. Comput. Methods Appl. Mech. Eng. **372**, 113382 (2020)